

Effect of counting chamber depth on the accuracy of lensless microscopy for the assessment of boar sperm motility

Carles Soler^{A,B,G}, José Á. Picazo-Bueno^C, Vicente Micó^C, Anthony Valverde^{A,D}, Daznia Bompert^B, Francisco J. Blasco^B, Juan G. Álvarez^{E,F} and Almudena García-Molina^B

^AUniversity of Valencia, Department of Cellular Biology, Functional Biology and Physical Anthropology, Campus Burjassot, C/ Dr Moliner, 50, 46100, Burjassot, Spain.

^BProiser R+D, C/ Catedràtic Agustín Escardino, 9, Building 3 (CUE), Floor 1, 46980, Paterna, Spain.

^CUniversity of Valencia, Department of Optics, Campus Burjassot, C/ Dr Moliner, 50, 46100, Burjassot, Spain.

^DTechnological Institute of Costa Rica, San Carlos Campus, School of Agronomy, 223-21001 Alajuela, Costa Rica.

^ECentro ANDROGEN, C/Fernando Macías 8-1°C, 15004, A Coruña, Spain

^FHarvard Medical School, Boston, MA, USA.

^GCorresponding author. Email: carles.soler@uv.es

Abstract. Sperm motility is one of the most significant parameters in the prediction of male fertility. Until now, both motility analysis using an optical microscope and computer-aided sperm analysis (CASA-Mot) entailed the use of counting chambers with a depth to 20 μm . Chamber depth significantly affects the intrinsic sperm movement, leading to an artificial motility pattern. For the first time, laser microscopy offers the possibility of avoiding this interference with sperm movement. The aims of the present study were to determine the different motility patterns observed in chambers with depths of 10, 20 and 100 μm using a new holographic approach and to compare the results obtained in the 20- μm chamber with those of the laser and optical CASA-Mot systems. The ISAS[®]3D-Track results showed that values for curvilinear velocity (VCL), straight line velocity, wobble and beat cross frequency were higher for the 100- μm chambers than for the 10- and 20- μm chambers. Only VCL showed a positive correlation between chambers. In addition, Bayesian analysis confirmed that the kinematic parameters observed with the 100- μm chamber were significantly different to those obtained using chambers with depths of 10 and 20 μm . When an optical analyser CASA-Mot system was used, all kinematic parameters, except VCL, were higher with ISAS[®]3D-Track, but were not relevant after Bayesian analysis. Finally, almost three different three-dimensional motility patterns were recognised. In conclusion, the use of the ISAS[®]3D-Track allows for the analysis of the natural three-dimensional pattern of sperm movement.

Additional keywords: CASA-Mot system, kinematic, laser.

Received 31 October 2017, accepted 7 March 2018, published online 4 May 2018

Introduction

Semen analysis is routinely used for the evaluation of male reproductive potential and the assessment of reproductive toxicity of environmental or therapeutic factors (Comhaire 1993; Guzick *et al.* 2001). For the most part, traditional semen analysis has been performed using subjective methods, such as light microscopy. In the case of human spermatozoa, such analyses have been defined by specific manuals from the World Health Organization (WHO 2010) and by the European Society for

Human Reproduction and Embryology (Barratt *et al.* 2011), two internationally recognised references.

The search for a more objective and accurate means of semen analysis led to the development of computer-aided sperm analysis (CASA) during the 1980s (Bompert *et al.* 2018). CASA-Mot systems based on optical two-dimensional (2D) microscopy analyse several kinematic parameters based on the position of the head centroid throughout the image sequence that was originally defined by Boyers *et al.* (1989). These

parameters, in addition to some introduced more recently, are used in most current CASA-Mot systems (Lu *et al.* 2014).

Although CASA systems have greatly improved the accuracy of semen analysis, this technology is based on optical microscopy. The depth of field, meaning the axial distance between the nearest and the furthest planes in which the sample appears in focus, is a limiting factor. The depth of field depends on the numerical aperture and magnification of the lens, and decreases when the wavelength of the illumination and the refractive index of the medium increase. For sperm motility studies, it is common to use $\times 10$ or $\times 20$ objectives, with a theoretical depth of the field of approximately 8.5 or 5.8 μm respectively (Amann and Waberski 2014).

The limitations of shallow counting chambers result in a 2D motility pattern that impedes the natural helical motion of the sperm tail. Considering that the length of the human spermatozoon is approximately 50 μm , more than 20 μm available space is needed to adequately measure sperm motility because it is considered to be helicoidal (Su *et al.* 2012). In the case of bull spermatozoa, it was established that tail helical movement is almost 25 μm in the z -axis (Rikmenspoel 1984) and so, taking into consideration the interactions with the glass surface (Woolley 2003; Elgeti *et al.* 2010; Lenz *et al.* 2011), the chamber depth should be almost 50 μm , which is beyond the capabilities of optical microscopy.

Another aspect to take into account is related to the use of phase contrast for the observation of moving spermatozoa (Zernike 1942a, 1942b; Shaked *et al.* 2012). Two alternatives are possible: positive and negative phase contrast. Positive phase contrast is only useful for some species (bull, camelids, human, stallion) with a three-dimensional (3D) elliptical shape, in which the sperm heads tend to be white in front of a more or less grey background, whereas background particles tend to be black. In other species (boar, goat, rabbit, ram), which present a flat lateral view, the use of positive phase contrast implies that the colour of the sperm heads varies from white to black, passing through all the possible grey grades, making it impossible to discriminate them correctly. Based on this, the alternative is to use negative phase contrast, in which sperm heads of all species appear nearly white against an almost black background. The problem with this optical technique is that the background particles also appear nearly white, introducing an overestimation of real concentration. In conclusion, negative phase contrast is better for the analysis of kinematics, whereas positive phase contrast is better for more accurate estimation of concentration values.

The development in the past decade of new microscopy technologies based on laser light and holographic analysis is opening a new spectrum of possibilities for the analysis of motility patterns in a 3D image using chambers with depths $> 100 \mu\text{m}$, thus solving the problems related to phase contrast (Su *et al.* 2012, 2013; Merola *et al.* 2013; Pushkarsky *et al.* 2014; Memmolo *et al.* 2015).

The main objectives of the present study were to use digital holographic microscopy (DHM) with the new CASA-Mot system ISAS[®]3D-Track to perform semen analysis to assess the effects of counting chamber depth on kinematic parameters of sperm motility, and to compare these results with those obtained using optical microscopy on ISAS[®]v1 CASA-Mot system.

Materials and methods

Sample preparation

Ten boar commercial insemination doses from Semen Cardona were received after conventional refrigerated transport (less than 24 h). After homogenisation of the doses, 1 mL was placed in an Eppendorf tube that was on an ISAS[®]PC12 heated plate (Proiser, precision 0.5°C) and maintained for 20 min at 37°C. Then, the semen samples were diluted with Acromax (Gestión Veterinaria Porcina) as described below. The counting chambers used were ISAS[®]D4C (Proiser) chambers with depths of 10, 20 and 100 μm and samples were diluted 1 : 2 for the ISAS v1 system (Proiser), whereas they were diluted 1 : 3 for 10 and 20- μm chambers and 1 : 5 for the 100- μm chambers used in the ISAS[®]3D-Track system (Proiser).

Optical CASA-Mot system: ISAS[®]v1

Kinematic analyses were performed using the ISAS[®]v1 CASA-Mot system, which consisted of a video camera (M03-ON High Speed 500 fps) attached to a microscope (UB203i; UOP/Proiser) equipped with $\times 10$ negative phase contrast objective. The resolution of the images analysed was 648 \times 488 pixels for a relationship of 0.755 μm per pixel in both axes. Samples were captured at 500 frame per second (f.p.s.) and videos were defragmented at 100 f.p.s. for comparison with images captured using the ISAS[®]3D-Track system. Analyses were performed according to the manufacturer's recommended set-up for boar semen. From each sample, seven fields (one for each square printed on the slide) were captured and analysed. CASA-Mot systems read a variety of kinematic parameters that were analysed and recorded in the study (Fig. 1).

Holographic CASA-Mot system: ISAS[®]3D-Track

The ISAS-3DTrack system prototype (Proiser; Fig. 2) was used in the present study. This system comprises a lensless holographic microscope, an automatically heated stage (at $37 \pm 0.5^\circ\text{C}$) and processing software. The lensless microscope is based on multi-illumination single-holographic-exposure lensless Fresnel (MISHELF) microscopy (Sanz *et al.* 2015, 2017) and is essentially a coherent imaging technique working without lenses where the digital sensor records a magnified and mis-focused hologram of the sample. The magnification comes from the geometric projection of the sample from the illumination source and is a factor of the distances in the device. However, it can easily be set to regular values in the range of $\times 10$ – 20 . In addition, the misfocus is a direct consequence of the lensfree configuration, yet, under certain approximations, numerical back-propagation to focus at the sample plane is possible. From the holographic images obtained, it is possible to generate phase contrast images or any other imaging modality without significantly increasing computational time.

A set of video movies was recorded with a digital sensor (Ximea Model MQ042CG-CM; Proiser) at a frame rate of 100 f.p.s. with a total duration of 1 s per video. Once the video movies were recorded, they entered a pipeline where the final result consisted of a focused image of the sperm cells moving along the recorded field of view. For the 10- and 20- μm chambers, all sperm cells appeared as focused by considering numerical

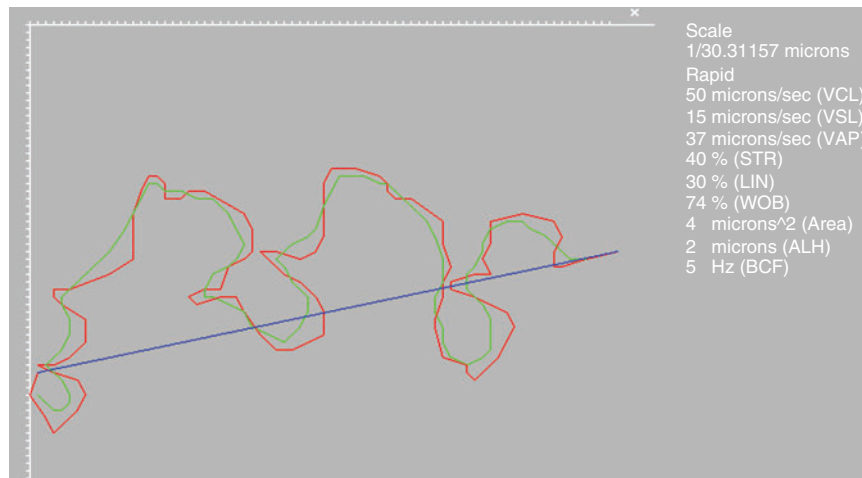


Fig. 1. Kinematic parameters as presented by the ISAS[®]v1 CASA system (Proiser). The red line shows curvilinear velocity (VCL), the blue line shows straight line velocity (VSL) and the green line shows average path velocity (VAP). STR, straightness ($=VSL/VAP \times 100$); LIN, linearity ($=VSL/VCL \times 100$); WOB, wobble ($=VAP/VCL \times 100$); ALH, amplitude of lateral head displacement; BCF, beat-cross frequency. In addition, we calculated mean dance as $VCL \times ALH$.



Fig. 2. The ISAS[®]3DTrack system prototype (Proiser).

propagation to a single plane. However, for the 100- μm chamber, there was a high number of planes containing some sperm cells in focus. The software is capable of tracking the 3D position of each analysed sperm cell in time and so that a full trajectory of the cell can be plotted and considered for computing all the parameters associated with the cell's 2D (by projection) and 3D kinematics.

In short, the x,y position of each spermatozoon was computed following local standard deviation minimisation criterion in a small region of interest (ROI) close to the cells: the x,y coordinates of spermatozoa were taken directly from the centroid positions of the head projections. The z coordinate was then added to this coordinate vector by taking into account the numerical propagation distance retrieved from the algorithm at the position where the x,y coordinates were set. Then, the x,y,z

coordinate vector was converted into a matrix by adding the temporal coordinate incoming from the frame number. Finally, the 3D trajectory of each spermatozoon could be constructed by linking the detected points across the recorded frames using conventional predicting tools (Kalman filters).

Statistical analysis

Classical analysis

To investigate the effects of chamber depth on sperm velocity, general linear models (GLM) were performed on all CASA-Mot parameters entered as response variables. Male number was entered as a fixed factor to control for individual variation. In each model, the dependent variable was the selected kinetic parameter (i.e. curvilinear velocity (VCL)) and the independent variable was the treatment. Data normality and homogeneity of variances were verified using Shapiro–Wilk normality tests and Levene's tests respectively. For CASA-Mot variables, a repeated-measures analysis of variance (ANOVA) was performed to determine whether differences were associated with depth (μm). Data are presented as the means \pm s.d. Pearson's correlations were performed between the CASA-Mot sperm parameters of motility of the different types of chambers. All statistical analyses were performed using InfoStat Software (v. 2017) for Windows (Di Rienzo *et al.* 2017). For all tests in the present study, statistical significance was accepted at two-tailed $P < 0.05$.

Bayesian analysis

Differences in sperm motility indicators were estimated with a model including the effect of chamber depth as a permanent effect. Male number was included as a random effect. All analyses were performed using Bayesian methodology. The posterior mean of the difference between chambers (D), the highest posterior density region at 95% (HPD_{95%}) and the

Table 1. Comparison of boar sperm kinematic parameters obtained with ISAS[®] 3D-Track using three counting chamber depths

Data are the mean \pm s.d. ($n = 4757$). Within rows, values with different superscript letters differ significantly ($P < 0.05$). D4C10, disposable ISAS[®] counting chamber with depth of 10 μm ; D4C20, disposable ISAS counting chamber with depth of 20 μm ; VCL, curvilinear velocity; VSL, straight line velocity; VAP, average path velocity; LIN, linearity; STR, straightness; WOB, wobble, ALH, amplitude of lateral head displacement; BCF, beat cross frequency; DM, medium dance

	D4C10	D4C20	Chamber depth 100 μm
Head area (μm^2)	26.91 \pm 8.53 ^a	26.68 \pm 9.20 ^a	25.46 \pm 8.75 ^b
VCL ($\mu\text{m s}^{-1}$)	114.43 \pm 45.88 ^a	121.75 \pm 52.35 ^b	155.52 \pm 47.57 ^c
VSL ($\mu\text{m s}^{-1}$)	30.94 \pm 19.61 ^a	33.41 \pm 22.30 ^b	59.27 \pm 28.84 ^c
VAP ($\mu\text{m s}^{-1}$)	37.11 \pm 19.70 ^a	37.86 \pm 18.66 ^a	56.23 \pm 19.43 ^b
LIN (%)	27.11 \pm 12.81 ^a	28.10 \pm 13.81 ^a	37.46 \pm 12.84 ^b
STR (%)	67.52 \pm 18.17 ^a	67.69 \pm 19.87 ^a	78.58 \pm 15.88 ^b
WOB (%)	38.70 \pm 11.19 ^a	39.87 \pm 11.78 ^b	46.58 \pm 9.93 ^c
ALH (μm)	1.25 \pm 0.48 ^a	1.22 \pm 0.48 ^a	1.34 \pm 0.43 ^b
BCF (Hz)	25.56 \pm 12.63 ^a	27.32 \pm 13.00 ^b	36.25 \pm 11.49 ^c
DM ($\mu\text{m}^2 \text{s}^{-1}$)	136.46 \pm 134.22 ^a	133.19 \pm 129.66 ^a	176.11 \pm 113.51 ^b

Table 2. Pearson's correlation analysis for boar sperm kinematic data between counting chamber depths

VCL, curvilinear velocity; VSL, straight line velocity; VAP, average path velocity; LIN, linearity; STR, straightness; WOB, wobble, ALH, amplitude of lateral head displacement; BCF, beat cross frequency

Variable	Chamber depths (μm)					
	100 vs 20 ($n = 1035$)		100 vs 10 ($n = 1714$)		20 vs 10 ($n = 1035$)	
	<i>r</i>	<i>P</i> -value	<i>r</i>	<i>P</i> -value	<i>r</i>	<i>P</i> -value
Head area	0.01	0.7539	0.01	0.5352	0.03	0.2959
VCL	0.87	<0.0001	0.91	<0.0001	0.89	<0.0001
VSL	0.33	<0.0001	0.33	<0.0001	0.19	<0.0001
VAP	0.42	<0.0001	0.46	<0.0001	0.28	<0.0001
LIN	-0.01	0.6623	-0.02	0.3997	3.3×10^{-3}	0.9165
STR	2.5×10^{-3}	0.9370	-0.04	0.1412	0.05	0.1287
WOB	-0.02	0.4645	2.7×10^{-3}	0.9114	0.03	0.4022
ALH	0.24	<0.0001	0.38	<0.0001	0.43	<0.0001
BCF	0.31	<0.0001	0.24	<0.0001	0.21	<0.0001

probability of the difference being positive when $D > 0$ or negative when $D < 0$ (P_0) were calculated. Bounded uniform priors were used for all effects. Residuals were *a priori* normally distributed with mean 0 and variance σ_e^2 . We considered one-third of the s.d. of a trait as a relevant value (R), and we also calculated the probability of relevance (P_R ; i.e. the probability of the difference being greater than R when $D > 0$ or lower than R when $D < 0$). The priors for the variances were also bounded uniform. Features of the marginal posterior distributions for all unknowns were estimated using Gibbs sampling. Convergence was tested using the *Z* criterion of Geweke (Sorensen and Gianola 2002) and Monte Carlo sampling errors were computed using time series procedures described in Geyer (1992). The Rabbit program, developed by the Institute for Animal Science and Technology (Valencia, Spain), was used for all procedures.

Results

Effects of counting chamber depth using ISAS[®] 3D-Track

There were no significant differences between the 10- and 20- μm chambers in values obtained for head area, average path

velocity (VAP), linearity (LIN), straightness (STR), amplitude of lateral head displacement (ALH) and medium dance (DM), but values were higher for VCL, straight line velocity (VSL), wobble (WOB) and beat cross frequency (BCF; Fig. 1). Values for all kinematic parameters were higher when the 100- μm chamber was used, with the exception of the head area, which was lower (Table 1).

There was no correlation between head area, LIN, STR and WOB values and different chambers depths, whereas there was a significant positive correlation for VSL, VAP, ALH and BCF with chamber depth, although *r* values were low; only VCL showed a strong positive correlation, with $r > 0.87$ (Table 2).

Bayesian analysis of the data showed that all variables exhibited relevant differences between the 100- μm chambers and the 10- and 20- μm chambers, with only ALH and DM exhibiting relevant differences between the 10- and 20- μm chambers (Table 3).

Differences between optical and laser CASA-Mot systems

Values for all kinematic parameters, except VCL, were higher when the ISAS[®] 3D-Track system was used (Table 4).

Table 3. Kinematic boar sperm parameters and estimated marginal posterior distributions of differences between chambers of different depth (n = 4757)

C₁, 100-µm deep chamber; C₂, 10-µm deep chamber; C₃, 20-µm deep chamber; D, mean of the marginal posterior distribution of the difference L - I, where L is ISAS3DTrack and I is ISASv1; HPD_{95%}, highest posterior density region at 95%; P₀, probability of the difference being greater than zero when D > 0, and lower than zero when D < 0; P_R, probability of the difference being greater than R when D > 0, and less than R when D < 0; VCL, curvilinear velocity; VSL, straight line velocity; VAP, average path velocity; LIN, linearity; STR, straightness; WOB, wobble, ALH, amplitude of lateral head displacement; BCF, beat cross frequency; DM, medium dance

	Mean ± s.d.	D	HPD _{95%}	P ₀	P _R
VCL (µm s ⁻¹)	134.41 ± 46.34				
C ₁ -C ₂		37.40	33.17, 41.23	1.00	1.00
C ₁ -C ₃		35.01	31.53, 38.51	1.00	1.00
C ₂ -C ₃		-2.39	-6.24, 1.38	0.89	0.00
VSL (µm s ⁻¹)	43.79 ± 22.63				
C ₁ -C ₂		24.54	22.58, 26.49	1.00	1.00
C ₁ -C ₃		25.16	23.48, 26.90	1.00	1.00
C ₂ -C ₃		0.61	-1.21, 2.45	0.74	0.00
VAP (µm s ⁻¹)	45.45 ± 17.50				
C ₁ -C ₂		17.26	15.77, 18.90	1.00	1.00
C ₁ -C ₃		18.07	16.76, 19.41	1.00	1.00
C ₂ -C ₃		0.81	-0.68, 2.22	0.86	0.00
LIN (%)	37.42 ± 12.38				
C ₁ -C ₂		8.43	7.36, 9.55	1.00	1.00
C ₁ -C ₃		8.99	8.00, 9.90	1.00	1.00
C ₂ -C ₃		0.55	-0.47, 1.59	0.85	0.00
STR (%)	80.88 ± 17.31				
C ₁ -C ₂		10.34	8.86, 11.93	1.00	1.00
C ₁ -C ₃		10.87	9.48, 12.15	1.00	1.00
C ₂ -C ₃		0.53	-0.90, 1.98	0.77	0.00
WOB (%)	51.23 ± 10.08				
C ₁ -C ₂		5.69	4.81, 6.56	1.00	1.00
C ₁ -C ₃		6.22	5.49, 7.01	1.00	1.00
C ₂ -C ₃		0.53	-0.29, 1.34	0.89	0.00
ALH (µm)	2.54 ± 0.43				
C ₁ -C ₂		0.12	0.08, 0.16	1.00	0.00
C ₁ -C ₃		0.14	0.11, 0.17	1.00	0.00
C ₂ -C ₃		0.02	-0.02, 0.05	0.83	0.00
BCF (Hz)	35.72 ± 11.78				
C ₁ -C ₂		10.50	9.50, 11.58	1.00	1.00
C ₁ -C ₃		9.21	8.31, 13.13	1.00	1.00
C ₂ -C ₃		-1.29	-2.31, -0.35	1.00	0.00
DM	152.02 ± 125.83				
C ₁ -C ₂		42.63	31.80, 52.47	1.00	0.56
C ₁ -C ₃		44.54	35.56, 53.45	1.00	0.72
C ₂ -C ₃		1.91	-7.94, 11.57	0.65	0.00
Head area (µm ²)	32.07 ± 8.71				
C ₁ -C ₂		-1.63	-2.37, -0.84	1.00	0.00
C ₁ -C ₃		-1.19	-1.89, -0.55	1.00	0.00
C ₂ -C ₃		0.43	-0.27, 1.17	0.88	0.00

There was no correlation in head area, LIN, STR and WOB between the two systems. There was a significant correlation between the two systems for VSL, VAP, ALH, BCF and DM, albeit with low r values, and only VCL showed a significant correlation with a high r value (r = 0.83; Table 5).

Table 4. Comparison of boar sperm kinematic parameters obtained with optical and laser CASA-Mot systems using a 20-µm deep counting chamber

Data are the mean ± s.d. (n = 4777). Within rows, different superscript letters indicate significant differences (P < 0.05). D4C: disposable ISAS counting chambers of 10 and 20 µm depth; VSL, straight line velocity; VAP, average path velocity; LIN, linearity; STR, straightness; WOB, wobble, ALH, amplitude of lateral head displacement; BCF, beat cross frequency; DM, medium dance

	ISAS [®] v1	ISAS [®] 3DTrack
Head area (µm ²)	28.68 ± 7.10 ^a	26.68 ± 9.20 ^b
VCL (µm s ⁻¹)	113.13 ± 40.82 ^a	121.75 ± 52.35 ^b
VSL (µm s ⁻¹)	39.07 ± 20.52 ^a	33.41 ± 22.30 ^b
VAP (µm s ⁻¹)	57.71 ± 22.27 ^a	37.86 ± 18.66 ^b
LIN (%)	34.10 ± 12.05 ^a	28.10 ± 13.81 ^b
STR (%)	72.62 ± 17.40 ^a	67.69 ± 19.87 ^b
WOB (%)	46.19 ± 9.58 ^a	39.87 ± 11.78 ^b
ALH (µm)	1.61 ± 0.47 ^a	1.22 ± 0.48 ^b
BCF (Hz)	26.43 ± 12.94 ^a	27.32 ± 13.00 ^b
DM (µm ² s ⁻¹)	199.34 ± 133.83 ^a	133.19 ± 129.66 ^b

Table 5. Pearson's correlation analysis between CASA-Mot systems for boar sperm kinematic data (n = 1714)

VSL, straight line velocity; VAP, average path velocity; LIN, linearity; STR, straightness; WOB, wobble, ALH, amplitude of lateral head displacement; BCF, beat cross frequency; DM, medium dance

Variable	r	P-value
Head area	0.03	0.2662
VCL	0.83	<0.0001
VSL	0.34	<0.0001
VAP	0.50	<0.0001
LIN	0.01	0.6576
STR	0.03	0.3008
WOB	0.02	0.4782
ALH	0.54	<0.0001
BCF	0.37	<0.0001
DM	0.58	<0.0001

Bayesian analysis of the data showed that even when significant differences were identified using classical probabilistic statistics, the differences between VCL, VSL, STR, BCF and head area should be considered non-relevant (Table 6).

3D sperm motility patterns

Several different 3D movement patterns were recognised, even though their kinematic values were not calculated. These included straight line horizontal patterns, patterns that changed in depth and circular patterns (Fig. 3).

The list of parameters that the system included were the classical CASA-Mot although calculated for the 3D-Track. In addition, rotation speed (revolutions per second (RPS)) was also calculated. The RPS represents the angular frequency of the linear function that best fits the temporal evolution of the rotation angle of the sperm head. Therefore, this new parameter

Table 6. Kinematic boar sperm parameters and estimated marginal posterior distributions of differences between CASA-Mot systems ($n = 4779$)
 D , mean of the marginal posterior distribution of the difference $L - I$, where L is ISAS3DTrack and I is ISASv1; $HPD_{95\%}$, highest posterior density region at 95%; P_0 , probability of the difference being greater than zero when $D > 0$, and lower than zero when $D < 0$; P_R , probability of the difference being greater than R when $D > 0$, and less than R when $D < 0$; VCL, curvilinear velocity; VSL, straight line velocity; VAP, average path velocity; LIN, linearity; STR, straightness; WOB, wobble, ALH, amplitude of lateral head displacement; BCF, beat cross frequency; DM, medium dance

	Mean \pm s.d.	D	$HPD_{95\%}$	P_0	P_R
Head area (μm^2)	27.45 \pm 7.79	-2.06	-2.56, -1.52	1	0.01
VCL ($\mu\text{m s}^{-1}$)	110.97 \pm 43.09	2.52	-0.39, 5.36	0.96	0
VSL ($\mu\text{m s}^{-1}$)	36.04 \pm 19.40	-7.47	-8.78, -6.16	1	0.71
VAP ($\mu\text{m s}^{-1}$)	45.44 \pm 19.26	-16.82	-18.16, -15.60	1	1
LIN (%)	33.63 \pm 12.04	-6.55	-7.33, -5.75	1	1
STR (%)	70.86 \pm 17.82	-3.71	-4.86, -2.52	1	0
WOB (%)	45.81 \pm 9.78	-7.61	-8.27, -6.95	1	1
ALH (μm)	1.36 \pm 0.46	-0.4	-0.43, -0.37	1	1
BCF (Hz)	26.77 \pm 12.03	0.42	-0.35, 1.25	0.85	0
DM ($\mu\text{m}^2 \text{s}^{-1}$)	155.59 \pm 129.00	-72.12	-81.05, -63.46	1	1

represents how fast or slow an evaluated helical trajectory revolves around its moving axis and its value is approximately half the BCF value.

Discussion

Semen analysis is the basic diagnostic tool for the determination of male fertility. It is essential in the andrological evaluation of human fertility and the fertilising potential of semen used in AI in farm animals. Although optical microscope-based CASA-Mot systems have demonstrated greater accuracy in motility assessment compared with subjective methods (Amann and Waberski 2014), these automated systems are not immune to artefacts in the measurement of sperm motility due to chamber depth and the evaluation of sperm morphology due to staining processes (Soler *et al.* 2016).

Commercial CASA-Mot systems allow the determination of multiple kinematic parameters (VSL, VCL, LIN etc.) including an in-plane focused image of the cells typically visualised under phase contrast microscopy or fluorescent imaging. However, CASA-Mot systems do not provide information for cells outside the focal plane. For this reason, standard counting chambers have a typical depth of 10–20 μm depending on the depth of field of the microscope lens and the selected application. Therefore, they are restricted by depth because only the in-focus cells are taken into account (Bompart *et al.* 2018).

As with most biological samples, spermatozoa are essentially transparent, appearing almost invisible under regular brightfield microscopy. However, they introduce a variation in the light phase in comparison with the surrounding medium incoming from a slightly higher refractive index value (Allen *et al.* 1995). Thus, classical phase contrast enhancement techniques (Zernike 1942a, 1942b; Hoffman and Gross 1975) and recent developments (Führhapter *et al.* 2005; Situ *et al.* 2010; Iglesias 2011) have enabled the qualitative visualisation of phase samples. Recently, quantitative characterisation of phase samples has become a reality because of the development of a wide range of techniques based on interferometric principles (Kim 2010; Popescu 2011; Shaked *et al.* 2012; Marquet *et al.* 2014; Majeed

et al. 2017). In particular, DHM has been demonstrated to be a powerful and versatile tool in sperm analysis, providing information regarding both the morphology and motility of sperm cells (Micó *et al.* 2010; Memmolo *et al.* 2011, 2015; Merola *et al.* 2013; Coppola *et al.* 2014; Di Caprio *et al.* 2015). DHM combines, into a single platform, high-quality imaging provided by microscopy, whole-object wavefront recovery provided by holography and numerical processing capabilities provided by computers (Micó *et al.* 2010).

DHM retrieves sample information and imaging through planes of focus by numerical refocusing of a single 2D holographic image at different depths of the whole object; therefore, a 3D environment is reconstructed, thus eliminating the need to restrict chamber depth to 20 μm . This enables the analysis of cells moving in a more natural fashion and in a more realistic 3D environment without being forced to creep within a thin chamber.

Within DHM there is an interesting discipline that is commonly referred as digital in-line holographic microscopy or lensless holographic microscopy (LHM). The idea is to remove the imaging lenses in the layout, thus simplifying it and reducing costs as well as dimensions. The concept was proposed by Hungarian physicist Dennis Gabor while working in the field of X-ray imaging during the 1940s (Gabor 1948) which led to the invention of holography. The idea was applied to the optical range a few years later (Rogers 1952) and upgraded to the digital domain at the beginning of the present century (Jericho *et al.* 2006; Repetto *et al.* 2004). Nowadays, LHM is a well-established technology with a considerable number of biomedical applications (Jericho *et al.* 2006; Heng *et al.* 2006; Cui *et al.* 2008; Frentz *et al.* 2010; Greenbaum *et al.* 2012; Perucho and Micó 2014; Sanz *et al.* 2015).

The results presented in this study constitute the first approach to the use of a commercial prototype based on LHM for the analysis of 2D tracks, comparing the values obtained using counting chambers with different depths and both optical-based and LHM-based CASA-Mot systems. LHM has enabled the definition of a new generation of cost-effective, lightweight,

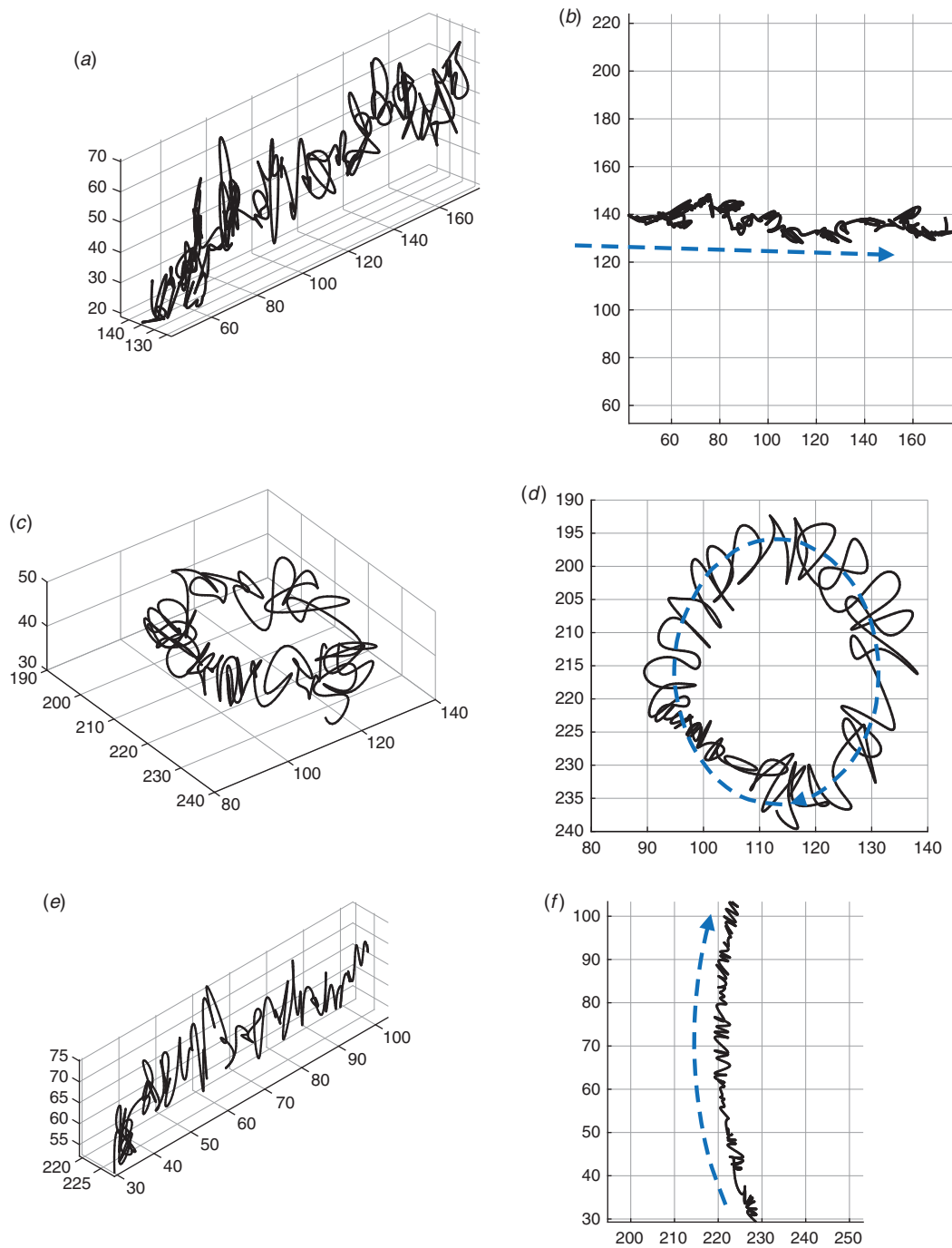


Fig. 3. Examples of (a, c, e) three-dimensional (3D) tracks and (b, d, f) their planar projections. (a, b) A cell with an almost straight line trajectory, but changing in z. (c, d) A cell with a circular trajectory. (e, f) A cell with a planar trajectory. Dashed blue arrows indicate the direction of movement.

compact and portable imaging platforms that greatly improve rapid and accurate diagnosis (Mudanyali *et al.* 2010a, 2010b; Isikman *et al.* 2011; Lee *et al.* 2011, 2014; Greenbaum *et al.* 2013; Pushkarsky *et al.* 2014; Sanz *et al.* 2017). In particular, LHM has been applied to sperm analysis, showing 3D trajectories of the sperm cells in a relatively deep (100 μm) counting

chamber (Sanz *et al.* 2017), revealing helical and twisted ribbon trajectories (Su *et al.* 2012, 2013).

Classical probabilistic statistics have shown that values for all the kinematic parameters increased with the depth of the counting chamber. Even between counting chambers with depths of 10 and 20 μm , the differences observed were

significant for some of kinematic parameters. When the 100- μm chamber was used, the increment was not only significant but $>11\%$ in all cases. When Bayesian statistics were used, only values of ALH, DM and head area showed relevant differences between the 10- and 20- μm chambers, whereas the observed differences were relevant in all cases when comparing the 100- μm chamber with the 10- and 20- μm chambers.

These results indicate that sperm cells show significant changes in their motility patterns when they move in a more natural fashion in a 3D setting without interference from glass surfaces.

Regarding the results of the comparison between optical and laser CASA-Mot systems, statistical analysis using a probabilistic approach showed differences between these two systems. This is due, in part, to the high number of cells analysed in each case. Looking at the relative variation, it was not so high. The fact that Bayesian statistics did not find relevant differences between both systems for VCL suggests that this new technology can be used indistinctly for the definition of boar sperm kinematics, and thus this new technique could be used for seminal dose calculation. Combining these results with the correlation analysis, it would be possible to establish a relationship between the data obtained in the past using the optic system and data corresponding to the new laser technology.

Considering that laser technology can also provide 3D analysis, we propose to introduce and define a new approach combining 2D and 3D information. Although data derived from the 3D analysis were not included in the present study, their inclusion in the future may provide important new information that could be used to obtain a more accurate definition of sperm cell movement (Su *et al.* 2012, 2013). It will also enable definition of sperm tail mechanics. However, the sperm tail, which is less than 1 μm in width, usually exhibits very weak light scattering, thus reducing the ability to analyse the sperm tail using holographic technology because it will likely be hidden by sperm head dynamics ($\sim 5 \mu\text{m}$ range, depending on species; for reviews, see Cummin and Woodall 1985; Yáñez *et al.* 2015).

Further applications

Residence in the cervical mucus is an important part in the process of sperm transport through the female reproductive tract in most mammals. However, the measurement of sperm motility inside the cervical mucus (Barratt *et al.* 1989), an inherently polydisperse and non-homogeneous material (Katz *et al.* 1978), is not possible with the use of the counting chambers currently used for semen motility analysis (depth up to 20 μm). In the natural medium of the cervical mucus, spermatozoa face variations in the microphysical environment that cannot be reproduced in the artificial low-viscosity media used for semen processing and analysis (Satake *et al.* 2006; van Gestel *et al.* 2007; Smith *et al.* 2009; Hunter *et al.* 2011; Olson *et al.* 2011). All the studies performed to date measuring sperm motility in the cervical mucus were based on subjective methods of analysis, and sperm motility in the cervical mucus could not be analysed using classical CASA-Mot systems (WHO 1992). This limitation resulted in the progressive disappearance of this test in standard human semen evaluation.

Quantitative information of the kinetics of sperm penetration and residence in the cervix and cervical mucus is available for humans (Sobrero and MacLeod 1962; Tredway *et al.* 1975; Katz *et al.* 1978; Ola *et al.* 2003) and other mammals (Morton and Glover 1974; Cox *et al.* 2002; Holt and Van Look 2004). In the case of humans, the three first editions of the WHO manual for semen analysis included the study of the interaction of semen with the cervical mucus (WHO 1992). Although it was assumed that progressive motility was a good indicator of cervical mucus penetration, progressive motility by itself ignores potential changes in sperm function within the cervical mucus environment. Unfortunately, this approach was time consuming and its presence in the literature has almost disappeared. In our opinion, this kind of functional approach offers interesting information that must be reconsidered for a better evaluation of sperm function.

In addition, the ability to perform 3D analysis at greater (counting chamber) depths will allow the study of the interactions between spermatozoa and oocytes in different species (Hay *et al.* 1997; McLeskey *et al.* 1997; Mengerink and Vacquier 2001; Nixon *et al.* 2007; Bobe and Labbé 2010).

Other important applications of the 3D CASA-Mot technology involve the study of chemotaxis in both research (Spehr *et al.* 2003; Böhmer *et al.* 2005) and clinical (Teves *et al.* 2006) settings. The use of high-depth chambers makes it possible to design future devices in which microfluidic movement can be defined (Knowlton *et al.* 2015; de Wagenaar *et al.* 2016).

Another potential application would be the evaluation of sperm hyperactivation during sperm capacitation (Yanagimachi 1970). This modality of sperm motility has been described in a great variety of mammals (Fraser 1977; Cummin 1982; Mortimer and Swan 1995a, 1995b) and may be involved in the final ascent of spermatozoa to the site of fertilisation in the tubal ampulla and/or in the generation of flagellar thrust required for cumulus and zona pellucida penetration (Morales *et al.* 1988). Classical optic CASA-Mot systems failed to provide correct evaluation of sperm hyperactivation because for real hyperactivated motility to be accurately measured, deep chambers should be used, thus allowing the sperm cells to have real movement, and a frame rate of almost 60 f.p.s. must be used (Mortimer and Swan 1995b). A recently published consensus between CASA-Mot users has emphasised the importance of using chambers with depth $\geq 30 \mu\text{m}$ to allow unconstrained flagellar movement for hyperactivation analysis (ESHRE Andrology Special Interest Group 1996). When hyperactivation was measured at 100 Hz, the observed beat frequency was $\leq 29.4 \text{ Hz}$, below the Nyquist number (where the frequency of the event must be less than half the frequency of the observations), indicating that the value obtained was not subject to aliasing (Mortimer *et al.* 1997). The use of chambers with a depth of 100 μm and a frame rate of 100 f.p.s., as demonstrated herein, opens up the possibility for a more accurate analysis of this sperm parameter.

In conclusion, the increase in counting chamber depth has a significant effect on sperm motility kinematic parameters, which become higher as chamber depth increases. Although the use of classical chambers for the optical microscope and

CASA-Mot systems (depths of 10 and 20 μm) results in similar values for most kinematic parameters, the introduction of 100- μm chambers results in a much higher speed, indicating a more natural cellular movement that is not affected by the glass surfaces. When counting chambers with depths of 10 and 20 μm were used, the differences for most of the kinematic parameters between optical and laser CASA-Mot systems were not relevant after Bayesian analysis. This means that the new 3D technology can be introduced for the routine analysis of boar semen in an equivalent manner to the way optical CASA-Mot systems have been used up to now. In addition, laser CASA-Mot systems offer a battery of new 3D parameters that could be used to improve our knowledge of sperm motility behaviour in different natural environments.

Conflicts of interest

The authors declare no conflicts of interest.

References

- Allen, M. J., Bradbury, E. M., and Balhorn, R. (1995). The natural subcellular surface structure of the bovine sperm cell. *J. Struct. Biol.* **114**, 197–208. doi:10.1006/JSBI.1995.1019
- Amann, R. P., and Waberski, D. (2014). Computer-assisted sperm analysis (CASA): capabilities and potential developments. *Theriogenology* **81**, 5–17.e3. doi:10.1016/J.THERIOGENOLOGY.2013.09.004
- Barratt, C. L. R., Osborn, J. C., Harrison, P. E., Monks, N., Dunphy, B. C., Lenton, E. A., and Cooke, I. D. (1989). The hypo-osmotic swelling test and the sperm mucus penetration test in determining fertilization on the human oocyte. *Hum. Reprod.* **4**, 430–434. doi:10.1093/OXFORDJOURNALS.HUMREP.A136922
- Barratt, C. L. R., Björndahl, L., Menkveld, R., and Mortimer, D. (2011). ESHRE Special Interest Group for Andrology basic semen analysis course: a continued focus on accuracy, quality, efficiency and clinical relevance. *Hum. Reprod.* **26**, 3207–3212. doi:10.1093/HUMREP/DER312
- Bobe, J., and Labbé, C. (2010). Egg and sperm quality in fish. *Gen. Comp. Endocrinol.* **165**, 535–548. doi:10.1016/J.YGCEN.2009.02.011
- Böhmer, M., Van, Q., Weyand, I., Hagen, V., Beyermann, M., Matsumoto, M., Hoshi, M., Hilderbrand, E., and Kaupp, U. B. (2005). Ca^{2+} spikes in the flagellum control chemotactic behaviour of sperm. *EMBO J.* **24**, 2741–2752. doi:10.1038/SJ.EMBOJ.7600744
- Bompart, D., García-Molina, A., Valverde, A., Caldeira, C., Yáñez, J., Núñez de Murga, M., and Soler, C. (2018). CASA-Mot technology: how results are affected for the frame rate and counting chamber. *Reprod. Fertil. Dev.* doi:10.1071/RD17551
- Boyers, S. P., Davis, R. O., and Katz, D. F. (1989). Automated semen analysis. *Curr. Probl. Obstet. Gynecol. Fertil.* **5**, 167–200.
- Comhaire, F. H. (1993). Methods to evaluate reproductive health of the human male. *Reprod. Toxicol.* **7**, 39–46. doi:10.1016/0890-6238(93)90067-H
- Coppola, G., Di Caprio, G., Wilding, M., Ferraro, P., Esposito, G., Di Matteo, L., Dale, R., Coppola, G., and Dale, B. (2014). Quantitative label-free animal sperm imaging by means of digital holographic microscopy. *IEEE J. Sel. Top. Quantum Electron.* **16**, 833–840.
- Cox, J. F., Zavala, A., Saravia, F., Rivas, C., Gallardo, P., and Alfaro, V. (2002). Differences in sperm migration through cervical mucus *in vitro* relates to sperm colonization of the oviduct and fertilizing ability in goats. *Theriogenology* **58**, 9–18. doi:10.1016/S0093-691X(02)00919-6
- Cui, X., Lee, L. M., Heng, X., Zhong, W., Sternberg, P. W., Psaltis, D., and Yang, C. (2008). Lensless high-resolution on-chip optofluidic microscopes for *Caenorhabditis elegans* and cell imaging. *Proc. Natl. Acad. Sci. USA* **105**, 10670–10675. doi:10.1073/PNAS.0804612105
- Cummins, J. M. (1982). Hyperactivated motility patterns of ram spermatozoa recovered from the oviducts of mated ewes. *Gamete Res.* **6**, 53–63. doi:10.1002/MRD.1120060107
- Cummins, J. M., and Woodall, P. F. (1985). On mammalian sperm dimensions. *J. Reprod. Fertil.* **75**, 153–175. doi:10.1530/JRF.0.0750153
- de Wagenaar, B., Dekker, S., de Boer, H. L., Bomer, J. G., Olthuis, W., van der Berg, A., and Segerink, L. I. (2016). Towards microfluidic sperm refinement: impedance-base analysis and sorting of sperm cells. *Lab Chip* **16**, 1514–1522. doi:10.1039/C6LC00256K
- Di Caprio, G., Ferrara, M. A., Miccio, L., Merola, F., Memmolo, P., Ferraro, P., and Coppola, G. (2015). Holographic imaging of unlabelled sperm cells for semen analysis: a review. *J. Biophotonics* **8**, 779–789. doi:10.1002/JBIO.201400093
- Di Rienzo, J. A., Casanoves, F., Balzarini, M. G., Gonzalez, L., Tablada, M., and Robledo, C. W. (2017). InfoStat versión 2017. (Grupo InfoStat, FCA, Universidad Nacional de Córdoba: Córdoba, Argentina.) Available at <http://www.infostat.com.ar> [verified 12 April 2018].
- Elgeti, J., Kaupp, U. B., and Gompper, G. (2010). Hydrodynamics of sperm cells near surfaces. *Biophys. J.* **99**, 1018–1026. doi:10.1016/J.BJP.2010.05.015
- ESHRE Andrology Special Interest Group (1996). Consensus workshop on advanced diagnostic andrology techniques. *Hum. Reprod.* **11**, 1463–1479. doi:10.1093/OXFORDJOURNALS.HUMREP.A019420
- Fraser, L. R. (1977). Motility patterns in mouse spermatozoa before and after capacitation. *J. Exp. Zool.* **202**, 439–444. doi:10.1002/JEZ.1402020314
- Frentz, Z., Kuehn, S., Hekstra, D., and Leibler, S. (2010). Microbial population dynamics by digital in-line holographic microscopy. *Rev. Sci. Instrum.* **81**, 084301. doi:10.1063/1.3473937
- Fürhapter, S., Jesacher, A., Bernet, S., and Ritsch-Marte, M. (2005). Spiral phase contrast imaging in microscopy. *Opt. Express* **13**, 689–694. doi:10.1364/OPEX.13.000689
- Gabor, D. (1948). A new microscopic principle. *Nature* **161**, 777–778. doi:10.1038/161777A0
- Geyer, C. (1992). Practical Markov chain Monte Carlo. *Stat. Sci.* **7**, 473–483. doi:10.1214/SS/1177011137
- Greenbaum, A., Luo, W., Su, T. W., Göröcs, Z., Xue, L., Isikman, S. O., Coskun, A. F., Mudanyali, O., and Ozcan, A. (2012). Imaging without lenses: achievements and remaining challenges of wide-field on-chip microscopy. *Nat. Methods* **9**, 889–895. doi:10.1038/NMETH.2114
- Greenbaum, A., Akbari, N., Feizi, A., Luo, W., and Ozcan, A. (2013). Field-portable pixel super-resolution colour microscope. *PLoS One* **8**, e76475. doi:10.1371/JOURNAL.PONE.0076475
- Guzick, D. S., Overstreet, J. W., Factor-Litvak, P., Brazil, C. K., Nakajima, S. T., Coutifaris, C., Carson, S. A., Cisneros, P., Steinkampf, M. P., Hill, J. A., Xu, D., Phil, M., and Vogel, D. L. (2001). Sperm morphology, motility and concentration in fertile and infertile men. *N. Engl. J. Med.* **345**, 1388–1393. doi:10.1056/NEJMOA003005
- Hay, M. A., King, W. A., Gartley, C. J., Leibo, S. P., and Goodrowe, K. L. (1997). Canine spermatozoa – cryopreservation and evaluation of gamete interaction. *Theriogenology* **48**, 1329–1342. doi:10.1016/S0093-691X(97)00374-9
- Heng, X., Erickson, D., Baugh, L. R., Yaqoob, Z., Sternberg, P. W., Psaltis, D., and Yang, C. (2006). Optofluidic microscopy – a method for implementing a high resolution optical microscope on a chip. *Lab Chip* **6**, 1274–1276. doi:10.1039/B604676B
- Hoffman, R., and Gross, L. (1975). Modulation contrast microscope. *Appl. Opt.* **14**, 1169–1176. doi:10.1364/AO.14.001169
- Holt, W. V., and Van Look, K. J. W. (2004). Concepts in sperm heterogeneity, sperm selection and sperm competition as biological foundations for laboratory tests of semen quality. *Reproduction* **127**, 527–535. doi:10.1530/REP.1.00134

- Hunter, R. H., Coy, P., Gadea, J., and Rath, D. (2011). Considerations of viscosity in the preliminaries to mammalian fertilization. *J. Assist. Reprod. Genet.* **28**, 191–197. doi:10.1007/S10815-010-9531-3
- Iglesias, I. (2011). Pyramid phase microscopy. *Opt. Lett.* **36**, 3636–3638. doi:10.1364/OL.36.003636
- Isikman, S. O., Bishara, W., Sikora, U., Yaglidere, O., Yeah, J., and Ozcan, A. (2011). Field-portable lensfree tomographic microscope. *Lab Chip* **11**, 2222–2230. doi:10.1039/C1LC20127A
- Jericho, S. K., Garcia-Sucerquia, J., Xu, W., Jericho, M. H., and Kreuzer, H. J. (2006). Submersible digital in-line holographic microscope. *Rev. Sci. Instrum.* **77**, 043706. doi:10.1063/1.2193827
- Katz, D. F., Mills, R. N., and Pritchett, T. R. (1978). The movement of human spermatozoa in cervical mucus. *J. Reprod. Fertil.* **53**, 259–265. doi:10.1530/JRF.0.0530259
- Kim, M. K. (2010). Principles and techniques of digital holographic microscopy. *SPIE Rev* **1**, 018005. doi:10.1117/6.0000006
- Knowlton, S. M., Sadasivam, M., and Tasoglu, S. (2015). Microfluidics for sperm research. *Trends Biotechnol.* **33**, 221–229. doi:10.1016/J.TIBTECH.2015.01.005
- Lee, M., Yaglidere, O., and Ozcan, A. (2011). Field-portable reflection and transmission microscopy based on lensless holography. *Biomed. Opt. Express* **2**, 2721–2730. doi:10.1364/BOE.2.002721
- Lee, S. A., Erath, J., Zheng, G., Ou, X., Willems, P., Eichinger, D., Rodriguez, A., and Yang, C. (2014). Imaging and identification of waterborne parasites using a chip-scale microscope. *PLoS One* **9**, e89712. doi:10.1371/JOURNAL.PONE.0089712
- Lenz, R. W., Kjelland, M. E., VonderHaar, K., Swannack, T. M., and Moreno, J. F. (2011). A comparison of bovine seminal quality assessments using different viewing chambers with a computer-assisted semen analyser. *J. Anim. Sci.* **89**, 383–388. doi:10.2527/JAS.2010-3056
- Lu, J. C., Huang, Y. F., and Lü, N. Q. (2014). Computer-aided sperm analysis: past, present and future. *Andrologia* **46**, 329–338. doi:10.1111/AND.12093
- Majeed, H., Sridharan, S., Mir, M., Ma, L., and Popescu, G. (2017). Quantitative phase imaging for medical diagnosis. *J. Biophotonics* **10**, 177–205. doi:10.1002/JBIO.201600113
- Marquet, P., Depeursinge, C., and Magistretti, P. J. (2014). Review of quantitative phase-digital holographic microscopy: promising novel imaging technique to resolve neuronal network activity and identify cellular biomarkers of psychiatric disorders. *Neurophotonics* **1**, 020901. doi:10.1117/1.NPH.1.2.020901
- McLeskey, S. B., Dowds, C., Carballada, R., White, R. R., and Sailing, P. M. (1997). Molecules involved in mammalian sperm–egg interaction. *Int. Rev. Cytol.* **177**, 57–113. doi:10.1016/S0074-7696(08)62231-7
- Memmo, P., Di Caprio, G., Distanti, C., Paturzo, M., Puglisi, R., Balduzzi, D., Galli, A., Coppola, G., and Ferraro, P. (2011). Identification of bovine sperm head for morphometry analysis in quantitative phase-contrast holographic microscopy. *Opt. Express* **19**, 23215–23226. doi:10.1364/OE.19.023215
- Memmo, P., Miccio, L., Paturzo, M., Di Caprio, G., Coppola, G., Netti, P. A., and Ferraro, P. (2015). Recent advances in holographic 3D particle tracking. *Adv. Opt. Photonics* **7**, 713–755. doi:10.1364/AOP.7.000713
- Mengerink, K. J., and Vacquier, V. D. (2001). Glycobiology of sperm–egg interactions in deuterostomes. *Glycobiology* **11**, 37R–43R. doi:10.1093/GLYCOB/11.4.37R
- Merola, F., Miccio, L., Memmolo, P., Di Caprio, G., Galli, A., Puglisi, R., Balduzzi, D., Coppola, G., Netti, P., and Ferraro, P. (2013). Digital holography as a method for 3D imaging and estimating the biovolume of motile cells. *Lab Chip* **13**, 4512–4516. doi:10.1039/C3LC50515D
- Micó, V., Ferreira, C., Zalevsky, Z., and García, J. (2010). Basic principles and applications of digital holographic microscopy. In ‘Microscopy: Science Technology, Applications and Education’. (Eds A. Méndez-Vilas and J. Diaz.) pp. 1411–1418. (Formatex Research Center: Badajoz, Spain.)
- Morales, P., Overstreet, J. W., and Katz, D. F. (1988). Changes in human sperm motion during capacitation *in vitro*. *J. Reprod. Fertil.* **83**, 119–128. doi:10.1530/JRF.0.0830119
- Mortimer, S. T., and Swan, M. A. (1995a). Variable kinematics of capacitating human spermatozoa. *Hum. Reprod.* **10**, 3178–3182. doi:10.1093/OXFORDJOURNALS.HUMREP.A135882
- Mortimer, S. T., and Swan, M. A. (1995b). Kinematics of capacitating human spermatozoa analysed at 60 Hz. *Hum. Reprod.* **10**, 873–879. doi:10.1093/OXFORDJOURNALS.HUMREP.A136053
- Mortimer, S. T., Schoëvaert, D., Swan, M. A., and Mortimer, D. (1997). Quantitative observations of flagellar motility of capacitating human spermatozoa. *Hum. Reprod.* **12**, 1006–1012. doi:10.1093/HUMREP/12.5.1006
- Morton, D. B., and Glover, T. D. (1974). Sperm transport in female rabbit: the rôle of the cervix. *J. Reprod. Fertil.* **38**, 131–138.
- Mudanyali, O., Oztoprak, C., Tseng, D., Erlinger, A., and Ozcan, A. (2010a). Quantitative observations of flagellar motility of capacitating human lensfree microscopy. *Lab Chip* **10**, 2419–2423. doi:10.1039/C004829A
- Mudanyali, O., Tseng, D., Oh, C., Isikman, S. O., Sencan, I., Bishara, W., Oztoprak, C., Seo, S., Khademhosseini, B., and Ozcan, A. (2010b). Compact, light-weight and cost-effective microscope based on lensless incoherent holography for telemedicine applications. *Lab Chip* **10**, 1417–1428. doi:10.1039/C000453G
- Nixon, B., Aitken, R. J., and McLaughlin, E. A. (2007). New insights into molecular mechanisms of sperm–egg interaction. *Cell. Mol. Life Sci.* **64**, 1805–1823. doi:10.1007/S00018-007-6552-X
- Ola, B., Afnan, N., Papioannou, S., Sharif, K., Bjorndahl, L., and Coomarasamy, A. (2003). Accuracy of sperm–cervical mucus penetration tests in evaluation sperm motility in semen: a systematic quantitative review. *Hum. Reprod.* **18**, 1037–1046. doi:10.1093/HUMREP/DEG209
- Olson, S. D., Suarez, S. S., and Fauci, L. J. (2011). Coupling biochemistry and hydrodynamics captures hyperactivated sperm motility in a simple flagellar model. *J. Theor. Biol.* **283**, 203–216. doi:10.1016/J.JTBI.2011.05.036
- Perucho, B., and Micó, V. (2014). Wavefront holography: application of digital in-line holography for the inspection of engraved marks in progressive addition lenses. *J. Biomed. Opt.* **19**, 16017. doi:10.1117/1.JBO.19.1.016017
- Popescu, G. (2011). ‘Quantitative Phase Imaging of Cells and Tissues.’ (McGraw-Hill Professional: New York.)
- Pushkarsky, I., Liu, Y., Weaver, W., Su, T. W., Mudanyali, O., Ozcan, A., and Di Carlo, D. (2014). Automated single-cell motility analysis on a chip using lensfree microscopy. *Sci. Rep.* **4**, 4717.
- Repetto, L., Piano, E., and Pontiggia, C. (2004). Lensless digital holographic microscope with light-emitting diode illumination. *Opt. Lett.* **29**, 1132–1134. doi:10.1364/OL.29.001132
- Rikmenspoel, R. (1984). Movements of bull sperm flagella as a function of temperature and viscosity. *J. Exp. Biol.* **108**, 205–230.
- Rogers, G. L. (1952). XIV. – Experiments in diffraction microscopy. *Proc. Roy. Soc. Edinburgh Sect. A* **63**, 193–221. doi:10.1017/S0080454100007093
- Sanz, M., Picazo-Bueno, J. A., García, J., and Micó, V. (2015). Improved quantitative phase imaging in lensless microscopy by single-shot multi-wavelength illumination using a fast convergence algorithm. *Opt. Express* **23**, 21352–21365. doi:10.1364/OE.23.021352
- Sanz, M., Picazo-Bueno, J. A., Granero, L., García, J., and Mico, V. (2017). Compact, cost-effective and field-portable microscope prototype based on MISHELF microscopy. *Sci. Rep.* **7**, 43291. doi:10.1038/SREP43291
- Satake, N., Elliott, R. M., Watson, P. F., and Holt, W. V. (2006). Sperm selection and activation in pigs may be mediated by the differential motility activation and suppression of sperm populations within the oviduct. *J. Exp. Biol.* **209**, 1560–1572. doi:10.1242/JEB.02136

- Shaked, N., Zalevsky, Z., and Satterwhite, L. L. (2012). 'Biomedical Optical Phase Microscopy and Nanoscopy.' (Elsevier: Amsterdam.)
- Situ, G., Warber, M., Pedrini, G., and Osten, W. (2010). Phase contrast enhancement in microscopy using spiral phase filtering. *Opt. Commun.* **283**, 1273–1277. doi:10.1016/J.OPTCOM.2009.11.084
- Smith, D. J., Gaffney, E. A., Gadêlha, H., Kapur, N., and Kirkman-Brown, J. C. (2009). Bend propagation in the flagella of migrating human sperm, and its modulation by viscosity. *Cell Motil. Cytoskeleton* **66**, 220–236. doi:10.1002/CM.20345
- Sobrero, A. J., and MacLeod, J. (1962). The immediate postcoital test. *Fertil. Steril.* **13**, 184–189. doi:10.1016/S0015-0282(16)34447-8
- Soler, C., Cooper, T. G., Valverde, A., and Yáñez, J. (2016). Afterword to *Sperm morphometrics today and tomorrow* special issue in *Asian Journal of Andrology*. *Asian J. Androl.* **18**, 895–897. doi:10.4103/1008-682X.188451
- Sorensen, D., and Gianola, D. (2002). 'Likelihood, Bayesian, and MCMC Methods in Quantitative Genetics.' 1st edn. (Springer-Verlag: New York.)
- Spehr, M., Gisselmann, G., Poplawski, A., Riffell, J. A., Wetzel, C. H., Zimmer, P. K., and Hatt, H. (2003). Identification of a testicular odorant receptor mediating human sperm chemotaxis. *Science* **299**, 2054–2058. doi:10.1126/SCIENCE.1080376
- Su, T.-W., Xue, L., and Ozcan, A. (2012). High-throughput lensfree 3D tracking of human sperms reveals rare statistics of helical trajectories. *Proc. Natl Acad. Sci. USA* **109**, 16018–16022. doi:10.1073/PNAS.1212506109
- Su, T.-W., Choi, I., Feng, J., Huang, K., McLeod, E., and Ozcan, A. (2013). Sperm trajectories form chiral ribbons. *Sci. Rep.* **3**, 1664. doi:10.1038/SREP01664
- Teves, M. E., Barbano, F., Guidobaldi, H. A., Sanchez, R., Miska, W., and Giojalas, L. C. (2006). Progesterone at the picomolar range is a chemoattractant for mammalian spermatozoa. *Fertil. Steril.* **86**, 745–749. doi:10.1016/J.FERTNSTERT.2006.02.080
- Tredway, D. R., Fordney-Settlage, D., Nakamura, R. M., Motoshima, M., Umezaki, C. U., and Mishell, R. D. (1975). Significance of timing for the postcoital evaluation of cervical mucus. *Am. J. Obstet. Gynecol.* **121**, 387–393. doi:10.1016/0002-9378(75)90018-6
- van Gestel, R. A., Brewis, I. A., Ashton, P. R., Brouwers, J. F., and Gadella, B. M. (2007). Multiple proteins present in the purified porcine sperm apical plasma membranes interact with the zona pellucida of the oocyte. *Mol. Hum. Reprod.* **13**, 445–454. doi:10.1093/MOLEHR/GAM030
- Woolley, D. M. (2003). Motility of sperm at surfaces. *Reproduction* **126**, 259–270. doi:10.1530/REP.0.1260259
- World Health Organization (WHO) (1992). 'WHO Laboratory Manual for the Examination of Human Semen and Sperm–Cervical Mucus Interaction.' 3rd edn. (Cambridge University Press: New York.)
- World Health Organization (WHO) (2010). 'WHO Laboratory Manual for the Examination and Processing of Human Semen.' 5th edn. (WHO: Switzerland)
- Yanagimachi, R. (1970). The movement of golden hamster spermatozoa before and after capacitation. *J. Reprod. Fertil.* **23**, 193–196. doi:10.1530/JRF.0.0230193
- Yáñez, J. L., Soler, C., and Santolaria, P. (2015). Computer assisted sperm morphometry in mammals: a review. *Anim. Reprod. Sci.* **156**, 1–12. doi:10.1016/J.ANIREPROSCI.2015.03.002
- Zernike, F. (1942a). Phase contrast, a new method for the microscopic observation of transparent objects Part I. *Physica* **9**, 686–698.
- Zernike, F. (1942b). Phase contrast, a new method for the microscopic observation of transparent objects Part II. *Physica* **9**, 974–986.